Physical Origin of the Differential Voltage Minimum Associated with Lithium Plating in Li-Ion Batteries

Journal of The Electrochemical Society, 2020 **167** 090540

Physical Origin of the Differential Voltage Minimum Associated with Lithium Plating in Li-Ion Batteries

Simon E. J. O'Kane,[1,2] Ian D. Campbell,[1] Mohamed W. J. Marzook,[1] Gregory J. Offer,[1,2,*] and Monica Marinescu[1,2,z]

[1]*Department of Mechanical Engineering, Imperial College London, United Kingdom*
[2]*The Faraday Institution, United Kingdom*

The main barrier to fast charging of Li-ion batteries at low temperatures is the risk of short-circuiting due to lithium plating. In-situ detection of Li plating is highly sought after in order to develop fast charging strategies that avoid plating. It is widely believed that Li plating after a single fast charge can be detected and quantified by using a minimum in the differential voltage (DV) signal during the subsequent discharge, which indicates how much lithium has been stripped. In this work, a pseudo-2D physics-based model is used to investigate the effect on Li plating and stripping of concentration-dependent diffusion coefficients in the active electrode materials. A new modelling protocol is also proposed, in order to distinguish the effects of fast charging, slow charging and Li plating/stripping. The model predicts that the DV minimum associated with Li stripping is in fact a shifted and more abrupt version of a minimum caused by the stage II-stage III transition in the graphite negative electrode. Therefore, the minimum cannot be used to quantify stripping. Using concentration-dependent diffusion coefficients yields qualitatively different results to previous work. This knowledge casts doubt on the utility of DV analysis for detecting Li plating.
 [DOI: 10.1149/1945-7111/ab90ac]

Manuscript submitted March 15, 2020; revised manuscript received April 24, 2020. Published May 18, 2020. *This paper is part of the JES Focus Issue on Battery Safety, Reliability and Mitigation.*

Supplementary material for this article is available online

List of symbols

± (subscript)	Denotes positive or negative electrode
$a_{\pm}$	Surface area to volume ratio of electrode, m^{-1}
c_a	Li^+ concentration in active material, mol m^{-3}
c_e	Li^+ concentration in electrolyte, mol m^{-3}
c_{eq}	Equilibrium Li^+ concentration in electrolyte, mol m^{-3}
c_{Li}	Concentration of plated Li, mol m^{-3}
$c_{m\pm}$	Maximum Li^+ concentration in active material, mol m^{-3}
c_s	Li^+ concentration at surface of active material, mol m^3
c_s^*	Normalized Li^+ concentration at surface, i.e., $c_s^* = \frac{c_s}{c_{m\pm}}$
$D_{\pm}$	Diffusion coefficient of active material, $m^2\ s^{-1}$
D_{eff}	Effective diffusion coefficient of electrolyte, $m^2\ s^{-1}$
F	Faraday's constant, C mol^{-1}
j_{tot}	Current per unit volume across interface, A m^{-3}
$k_{\pm}$	Rate constant for main (de)intercalation reaction, m s^{-1}
k_{sr}	Rate constant for plating/stripping, m s^{-1}
M_{Li}	Molar mass of Li metal, kg mol^{-1}
N_{int}	Net deintercalation flux across interface, mol $m^{-2}\ s^{-1}$
N_{sr}	Net stripping flux across interface, mol $m^{-2}\ s^{-1}$
Q	Discharge capacity, mAh
Q_{Li}	Total capacity of plated Li, mAh
Q_{nom}	Nominal capacity, mAh
R	Universal gas constant, J K^{-1} mol^{-1}
$r_{\pm}$	Electrode particle radius, m
r	Distance from particle centre, m
T	Absolute temperature, K
t	Time from beginning of simulation, s
t^+	Li^+ Transference number
$U_{\pm}$	Open-circuit potential, V
V	Cell voltage, V
V_{max}	Upper cutoff voltage, V
V_{min}	Lower cutoff voltage, V
x	Distance from negative current collector, m
$\delta_{\pm}$	Electrode thickness, m
ϵ	Electrolyte volume fraction
η	Overpotential for main (de)intercalation reaction, V
κ_{eff}	Effective electrolyte conductivity, S m^{-1}
ρ_{Li}	Density of Li metal, kg m^{-3}
$\sigma_{\pm}$	Electrode conductivity, S m^{-1}
ϕ_e	Electrolyte potential with respect to Li/Li^+, V
ϕ_s	Electrode potential with respect to Li/Li^+, V

The various problems associated with fast charging of Li-ion batteries form one of several barriers to large-scale use of electric vehicles.[1] The most intensively researched of these problems is lithium (Li) plating on the graphite negative electrode.[2,3]

Lithium plating is a Faradaic side reaction where Li^+ ions from the electrolyte form Li metal on the surface of the negative electrode instead of intercalating into it.[4] This reaction mainly occurs during fast charging when the electrostatic potential of the negative electrode approaches or falls below that of a Li/Li^+ reference electrode.[5] It is aggravated by factors that slow down the competing intercalation reaction, including low temperatures[6] and insufficient negative electrode material into which to insert lithium.[7,8]

As with any electroplating reaction, the Li metal can be recovered through the inverse reaction, known as stripping. However, Li metal quickly undergoes further side reactions with the electrolyte to form SEI.[4,5,9] This SEI growth can electrically isolate the remaining Li, forming "dead lithium" and preventing its recovery.[10,11] Both additional SEI growth and isolated lithium cause loss of lithium inventory and reduce conductivity through pore clogging[4,12] and solvent evaporation, but Li plating also poses a safety risk in the formation of dendrites, which can short-circuit the cell causing rapid heating.[13]

For this reason, reliable in situ methods of identifying and quantifying Li plating are highly sought after. Zhang et al.[14] presented three methods of quantifying capacity loss due to irreversible Li plating over many cycles: Arrhenius plots, as previously reported by Waldmann et al.,[15] resistance-capacity plots and mean capacity fade per cycle. Zhang et al. found all three methods to test positively for plating for cells subjected to low temperature fast charging, negatively for cells with slow charging and high temperatures and inconclusively for intermediate scenarios.

*Electrochemical Society Member.
[z]E-mail: monica.marinescu@imperial.ac.uk

In order to prevent short-circuiting, however, it is necessary to be able to quantify the Li plating due to a single fast charge. Smart et al.[16] identified a high voltage plateau at the beginning of discharge that appears to be characteristic of Li stripping. Petzl and Danzer[17] used differential voltage (DV) analysis to identify the end of the voltage plateau. Petzl and Danzer assumed this minimum marks the end of the stripping process and therefore used the capacity at which the minimum occurs to estimate the amount of reversibly plated Li. To find out if this is indeed the case, simulations of Li plating and stripping are required.

Building on the earlier modelling work of Arora, Doyle and White,[5] Yang et al.[18] and Ren et al.[19] compared experimental and simulated DV analyses. They found that in the simulations, most or all of the Li is indeed stripped at the capacity at which the minimum occurs. Zhao et al.[20] also compared experimental and simulated DV analyses; unlike Yang et al. and Ren et al., their model included the second irreversible reaction where plated Li reacts with the electrolyte to form SEI. They found that for higher discharge rates, more of the plated Li could be recovered, implying the plated Li capacity was calculated, but no plots of plated Li capacity were included.

However, most DV analyses of fast charging in the literature do not make any attempt to distinguish the effects of fast charging from other effects, such as phase transitions between different stages of lithiation in graphite. Campbell et al.[6] conducted control studies of discharge after a slow charge—which they termed "reference discharges"—and found two DV minima early in the discharge. One minimum occurred within the first 150 mAh of discharge (out of a total capacity of 7.5 Ah), only when the cell was conductively cooled, and not when the cell was convectively cooled in a thermal chamber. The second minimum occurred around 1 Ah for both cooling methods and was observed for the reference discharges as well as after the fast charge. Since the second minimum also occurred after a slow charge, it could not be caused by plating. Instead, this second minimum is consistent with the DV signal resulting from one of the graphite stage changes. According to the theory that the DV minimum marks the end of stripping, no plating is expected to take place in the convectively cooled cells. However, cell teardowns confirmed Li plating had occurred for both cooling methods, leading Campbell et al. to conclude, "absence of evidence is not evidence of absence."

The other main problem in the current literature is on the modelling side and concerns the assumptions made around the diffusion coefficient of Li^+ inside the graphite particles. Measurements[21,22] and modelling[23,24] have shown that the diffusion coefficient is high for concentrations at which graphite undergoes phase transitions between stages of lithiation and low for other concentrations. However, most models neglect the dependence of diffusion coefficient on Li^+ concentration altogether,[5,19,20] while Yang et al.[18] assume a simple power law with no dependence on staging. Given the large concentration gradients within the graphite particles after a fast charge, this oversimplified treatment of Li^+ diffusion is a major limitation.

In this work, concentration-dependent diffusion coefficients and control studies of the type performed by Campbell et al.[6] are combined for the first time. The work of Yang et al.[18] is extended to include more realistic diffusion coefficients and reduce the number of adjustable parameters. Parameters - including concentration-dependent diffusion coefficients - for the cells used by Campbell et al. have already been obtained,[22,25] enabling direct comparison with Campbell et al.'s results while minimizing the potential for overfitting. By performing different simulations and directly comparing the results with Campbell et al.'s experiments, the effects of fast charging, slow charging and concentration-dependent diffusion coefficients on Li plating can be distinguished.

Theory

The model in this work is largely based on that of Yang et al.,[18] with differences in the implementation and the equation for Li plating/stripping. The pseudo-2D model of Li-ion batteries was developed by Fuller, Doyle and Newman[26] and solves for four scalar fields: electrostatic potential $\phi_e(x, t)$ in the electrolyte, electrostatic potential $\phi_s(x, t)$ in the solid-phase electrode particles, electrolyte concentration $c_e(x, t)$ and concentration $c_a(x, r, t)$ of Li^+ in the active material of the electrode particles. These fields are found by solving four differential equations. Charge conservation in the solid electrode particles is given by Ohm's law:

$$\sigma_{\pm}\frac{\partial^2\phi_s}{\partial x^2} = j_{tot}, \quad [1]$$

where $\sigma_{\pm}$ is the conductivity of the solid particles in the positive or negative electrode, which is denoted by an $+$ or $-$ subscript respectively, and j_{tot} is the current per unit volume across the interface between the solid electrode particles and the electrolyte. The equivalent equation for the electrolyte has both Ohmic and non-Ohmic terms:

$$-\kappa_{eff}(c_e, T)\frac{\partial^2\phi_e}{\partial x^2} + \frac{2RT}{F}\kappa_{eff}(c_e, T)(1 - t^+)\frac{\partial^2 \ln c_e}{\partial x^2} = j_{tot}, \quad [2]$$

where $\kappa_{eff}(c_e, T)$ is the effective conductivity of the electrolyte, T is the cell temperature, R is the universal gas constant, F is Faraday's constant and t^+ is the transference number of Li^+ ions in the electrolyte. Similarly, the continuity equation in the electrolyte has diffusion and source terms:

$$\frac{\partial(\epsilon c_e)}{\partial t} = \frac{\partial}{\partial x}\left(D_{eff}(c_e, T)\frac{\partial c_e}{\partial x}\right) + \left(\frac{1 - t^+}{F}\right)j_{tot}, \quad [3]$$

where ϵ is the electrolyte volume fraction - also referred to as the porosity—and $D_{eff}(c_e, T)$ is the effective diffusion coefficient of the electrolyte. The continuity equation in the electrode particles accounts for diffusion in the radial dimension r of spherical particles:

$$\frac{\partial c_a}{\partial t} = \frac{1}{r^2}\frac{\partial}{\partial r}\left(D_{\pm}(c_a, T)r^2\frac{\partial c_a}{\partial r}\right), \quad [4]$$

with the source term as a boundary condition:

$$D_{\pm}(c_a, T)\frac{\partial c_a}{\partial x}\bigg|_{r=r_{\pm}} = -N_{int}(x, t). \quad [5]$$

The diffusion coefficient $D_{\pm}(c_a, T)$ in the electrode particles is usually the main rate-limiting factor for high charge/discharge rates and is therefore a critical parameter. The current per unit volume j_{tot} across the electrode-electrolyte has contributions from the main Li^+ intercalation/deintercalation reaction and the Li plating/stripping side reaction:

$$j_{tot} = Fa_{\pm}(N_{int} + N_{sr}), \quad [6]$$

where $a_{\pm}$ is the surface area to volume ratio of the electrode and N_{int} and N_{sr} are the net reaction fluxes per unit area for deintercalation and stripping respectively (negative values correspond to intercalation and plating). Both fluxes are calculated using Butler–Volmer equations. The Butler-Volmer equation for the main reaction flux N_{int} is well known:

$$N_{int} = 2k_{\pm}(T)\sqrt{\frac{c_e}{c_{eq}}(c_{m\pm} - c_s)c_s}\sinh\left(\frac{F\eta}{2RT}\right), \quad [7]$$

where $k_{\pm}(T)$ is the reaction rate constant, c_{eq} is the electrolyte concentration at equilibrium, $c_{m\pm}$ is the maximum Li^+ concentration in the active material, $c_s(x, t) = c_a(x, r = r_{\pm}, t)$ is the concentration of Li^+ at the surface of the electrode particles and the reaction overpotential η is defined with respect to the open-circuit potential $U_{\pm}(c_s)$:

$$\eta = \phi_s - \phi_e - U_{\pm}(c_s). \quad [8]$$

The SEI resistance has not been included in 8 as measuring this would require impedance spectroscopy measurements on these particular cells; this data is not available in Campbell et al.[6] The first Butler-Volmer equation for Li plating/stripping was devised by Arora, Doyle and White[5] and assumed a constant exchange current density with no dependence on the electrolyte concentration c_e or the concentration c_{Li} of plated Li. Yang et al.[18] used an updated equation that included concentration dependence:

$$N_{sr} = k_{sr}(c_{Li}^*)^{\alpha_{c,Li}}(c_e^*)^{\alpha_{a,Li}}\left(\frac{c_{Li}}{c_{Li}^*}\exp\left(\frac{\alpha_{a,Li}F}{RT}(\phi_s - \phi_e)\right) - \frac{c_e}{c_e^*}\exp\left(-\frac{\alpha_{c,Li}F}{RT}(\phi_s - \phi_e)\right)\right), \quad [9]$$

where $c_e^* = c_{eq}$ and both k_{sr} and c_{Li}^* were used as fitting parameters. The transfer coefficients $\alpha_{a,Li}$ and $\alpha_{c,Li}$ were set to 0.3 and 0.7 respectively, as Arora, Doyle and White[5] did, citing a study by Verbrugge and Koch.[27] However, Wood et al.[28] assume $\alpha_{a,Li} = \alpha_{c,Li} = 0.5$, citing a different paper by Verbrugge and Koch.[29] More recent measurements suggest $\alpha_{a,Li}$ and $\alpha_{c,Li}$ to be approximately 0.4 and 0.6 respectively.[30–32] Given the large spread of values in the literature, the null hypothesis of a symmetrical reaction with $\alpha_{a,Li} = \alpha_{c,Li} = 0.5$ is assumed in this work. It is also worth noting that reference concentrations are arbitrary, therefore 9 remains valid if $c_{Li}^* = c_e^* = c_{eq}$, resulting in both reference concentrations disappearing. Making both of these changes results in a simpler equation for Li plating/stripping while retaining full concentration dependence:

$$N_{sr} = k_{sr}\left(c_{Li}\exp\left(\frac{F(\phi_s - \phi_e)}{2RT}\right) - c_e\exp\left(-\frac{F(\phi_s - \phi_e)}{2RT}\right)\right). \quad [10]$$

Equation 10 is identical to the equation for Li plating/stripping used by Wood et al.,[28] although they were modelling Li metal electrodes rather than plating on graphite. The main reason for using it, however, is that k_{sr} is now the only fitting parameter. Since the concentration c_{Li} of an additional species is introduced, an additional continuity equation is required, which is given by Yang et al.[18]:

$$\frac{\partial c_{Li}}{\partial t} = -a_- N_{sr}. \quad [11]$$

The effect of plating/stripping on the porosity $\epsilon(x, t)$ is also accounted for using the method of Sikha, Popov and White[33]:

$$\frac{\partial \epsilon}{\partial t} = a_- \frac{M_{Li}}{\rho_{Li}} N_{sr}. \quad [12]$$

One major difference between this and similar models[18–20] is the lack of any thermal modelling. Instead, for simplicity in the present work, the cell temperature is a function of time based on experimental measurements. This approach avoids the need to find parameters for the thermal model, which were not provided by Ecker et al.,[22,25] so more effort can be directed into investigating the effects of changing the plating/stripping rate constant k_{sr} and graphite diffusion coefficient $D_-(c_a, T)$. However, the experimental measurements do not account for thermal gradients in the cell.

Experimental

All experimental work in this paper has been presented previously by Campbell et al.,[6] so only a brief summary is given here. Testing was performed on two commercially available high-energy Kokam 7500 mAh (nominal capacity Q_{nom}) cells with model number SLPB75106100. Although nominally NMC-Graphite, Ecker et al.[22] used Inductively Coupled Plasma Optical Emission Spectroscopy (ICP-OES) to find the positive electrode to be made of $LiNi_{0.4}Co_{0.6}O_2$, i.e., NMC406. Charging at up to 1C (1.8 mA cm^{-2}) between 273.15 K (0 °C) and 313.15 K (40 °C) is approved by the manufacturer, while lower and upper voltage cutoffs are 2.7 V (V_{min}) and 4.2 V (V_{max}) respectively.

Two different thermal management systems were used. One cell was conductively cooled using a water/propylene glycol (1:1) coolant maintained at 273.15 K. The other cell was placed in a binder with an ambient temperature at the same value of 273.15 K and was therefore cooled by natural air convection. The surface temperature of the cells was measured using type K thermocouples with an accuracy of ±1.5 K.

Charge-discharge cycling was conducted using a battery cycler (Bio-Logic, BCS-815). Both cells were initially discharged at C/5 (0.4 mA cm^{-2}) to V_{min}, allowed 1 h to equilibrate, then subjected to a CCCV charge consisting of a constant current charge at C/10 (0.2 mA cm^{-2}) to V_{max} followed by a constant voltage charge until current $I <$ C/20 (0.1 mA cm^{-2}) to evaluate capacity. As a control study, cells were recharged to 80% state of charge (SoC) at a reference rate of C/10 (the "reference charge") and immediately discharged at C/20 to V_{min} (the "reference discharge"). Following 1 h of equilibration, cells were subjected to a fast CCCV charge consisting of a 4C (7.3 mA cm^{-2}) constant current charge to V_{max} followed by a constant voltage charge to 80% SoC, then immediately discharged at C/20 to V_{min} (the "stripping discharge").

Simulations

Simulations were conducted in COMSOL 5.3a using the Batteries and Fuel Cells module to implement the equations in the Theory section . The cells used in the experiments have the same model number as the 7500 mAh (Q_{nom}) cell parameterized by Ecker et al.,[22,25] so most of the parameters used in this work were taken from those papers. The empirical functions for the open-circuit potential $U_-(c_s)$ and diffusion coefficient $D_-(c_a)$ of the negative electrode are particularly important when studying Li plating/stripping, so these are plotted in Figs. 1a and 1b respectively. Note the dependence of these quantities on the various stages of lithiation, which is consistent with reports elsewhere in the literature.[21,23,24] All other parameters are given in the Supplementary Information available online at stacks.iop.org/JES/167/090540/mmedia. Two parameters had to be modified. The capacity loss due to initial SEI formation had to be increased from 6.8% to 10.4% (halfway between Ecker et al.'s fitted and measured values) for the experimental and simulated cell capacities to match during the reference discharge. The inactive fraction in the negative electrode was also increased from 44.5% to 50% to align the reference discharge DV signal to the measurements of Campbell et al.[6] The only relevant parameters not found by Ecker et al. were those specific to Li plating/stripping. The molar mass M_{Li} and density ρ_{Li} of Li metal are known to be 0.00694 kg mol^{-1} and 534 kg m^{-3} respectively, while the plating/stripping rate constant k_{sr} was treated as a temperature-independent fitting parameter for which multiple values were investigated.

The experimental charge/discharge protocol was replicated as closely as possible in the simulations. The cell began in the fully charged equilibrium state calculated by Ecker et al.[25] and was discharged at C/20 (0.1 mA cm^{-2}) to $V_{min} = 2.7$ V and left to equilibrate for 1 h, as an approximation to the fully discharged state. The reference charge to 80% state of charge (SoC) at C/10 (0.2 mA cm^{-2}) was then conducted, followed immediately by the reference discharge to V_{min} at C/20. The point at which 80% SoC was reached was determined by integrating the current over time. Following another 1 h equilibration, a fast CCCV charge, consisting of a 4C (7.3 mA cm^{-2}) constant current charge to $V_{max} = 4.2$ V followed by a constant voltage charge to 80% SoC, was conducted. After the fast charge the Li^+ concentration at the surface of the graphite particles approaches its maximum value (i.e., $c_s \approx c_{m-}$)

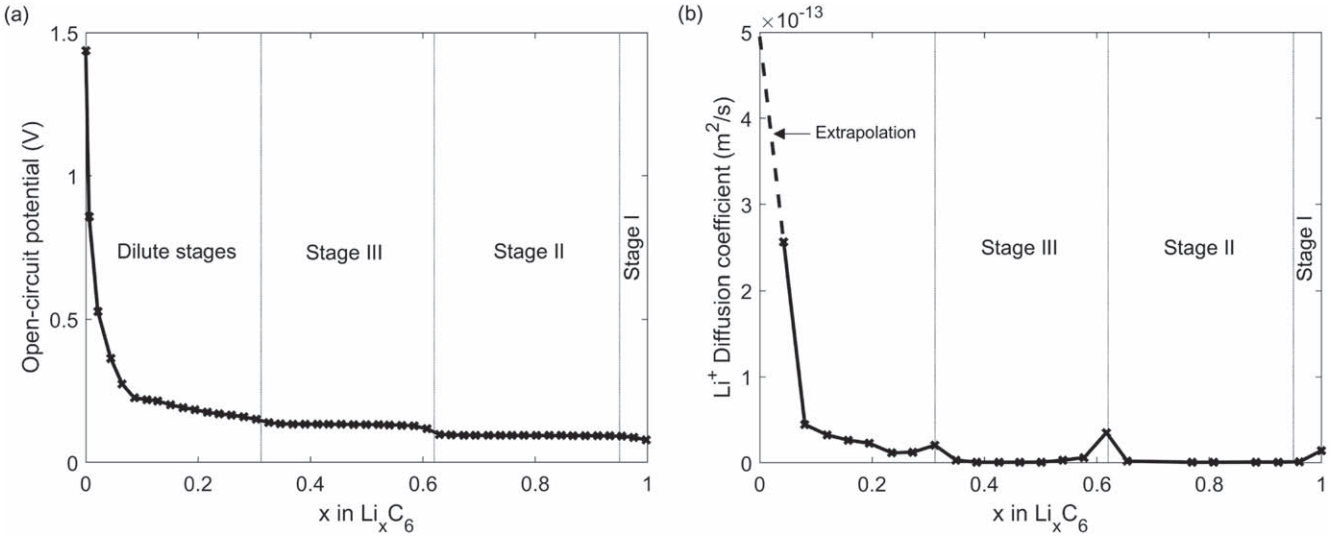

Figure 1. (a) Open-circuit potential and (b) Li^+ diffusion coefficient in the graphite negative electrode as a function of normalized Li^+ concentration, as measured by Ecker et al.[22] at 296 K.

making the numerical solution unstable, so 20 s of equilibration between the fast charge and stripping discharge was necessary to avoid unphysical positive values for the differential voltage $\frac{dV}{dQ}$ at the beginning of discharge. The stripping discharge was done at a rate of C/20 to V_{min}, as with the reference discharge.

In order to investigate why the first DV minimum was observed for conductive cooling but not for convective cooling, both cooling methods were simulated. Figure 2 shows the experimentally measured surface temperature of the conductively cooled and convectively cooled cells, during both the fast charge and stripping discharge.[6] For the conductively cooled cell, the experimental surface temperature varied by no more than 3 K (the uncertainty on the measurements was ±1.5 K) throughout the cycle, so the temperature was kept constant at 273.15 K throughout the simulation. For the convectively cooled cell, the simulated temperature was kept at the same constant value $T_{init} = 273.15$ K during the initialization, reference charge, reference discharge and 1 h equilibration, but became a time-varying function

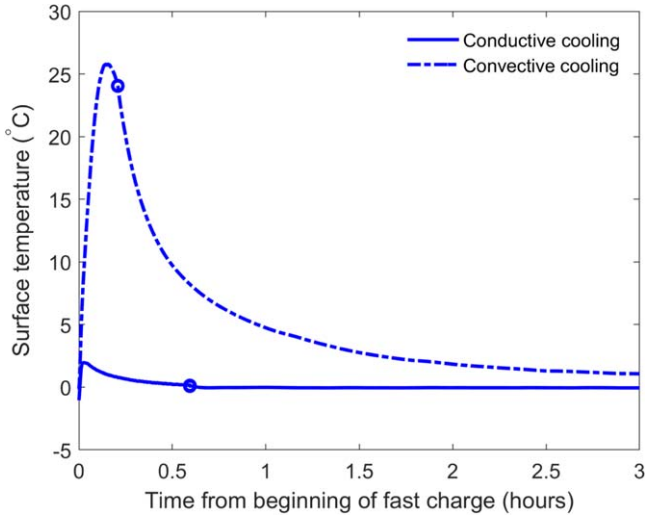

Figure 2. Experimentally measured surface temperature of the conductively cooled and convectively cooled cells, as functions of time, from Campbell et al.[6] The circles indicate the end of charge and beginning of discharge.

$$T_{rise}(t) = T_{init} + \Delta T\left[1 - \exp\left(-\frac{t - t_{BoC}}{t_{rise}}\right)\right] \quad [13]$$

during the fast CCCV charge and

$$T_{fall}(t) = T_{init} + \Delta T \exp\left(-\frac{t - t_{EoC}}{t_{fall}}\right) \quad [14]$$

during the 20 s equilibration and stripping discharge, where $\Delta T = 25$ K, t_{BoC} is the time at which the CC charge begins, $t_{rise} = 300$ s, t_{EoC} is the time at which the CV charge ends and $t_{fall} = 1920$ s, based on the data in Fig. 2. The main effect of varying the temperature is through the strong Arrhenius dependence on T of the (de)intercalation rate constants $k_{\pm}(T)$ and diffusion coefficients $D_{\pm}(c_a, T)$, as detailed in the Supplementary Information.

Results and Discussion

Figures 3a and 3b show experimentally measured voltage-capacity plots for both reference and stripping discharges for the (a) conductively cooled and (b) convectively cooled cells.[6] For both cells, the stripping discharge begins with a high voltage plateau whereas the reference discharge does not, although the plateau lasts significantly longer for the conductively cooled cell. After the voltage plateau ends, the reference and stripping discharges are mostly identical, except for the end of discharge for the convectively cooled cell, where there appears to be an increase in discharge capacity after the fast charge. Campbell et al.[6] noted that this effect has previously been observed by Gyenes et al.,[34] who proposed that the extra capacity could be due to Li^+ in the overhang, at the edges of the negative electrode, becoming active.

Figures 3c and 3d show differential voltage (DV) plots for the (c) conductively cooled and (d) convectively cooled cells. To remove noise from the DV plots, the voltage data was smoothed before differentiating using the moving average method, a window of 0.5% of the data and 2 iterations. For both cells, the reference and stripping discharges have very different DV signals at the start of discharge but converge after about 1500 mAh. Panels (e) and (f) show the same DV plots but zoomed in to show the first 1200 mAh of discharge. For the conductively cooled cell, the DV signal for the stripping discharge has a minimum at 140 mAh, which is similar to the DV minimum observed by Petzl and Danzer[17] during a similar

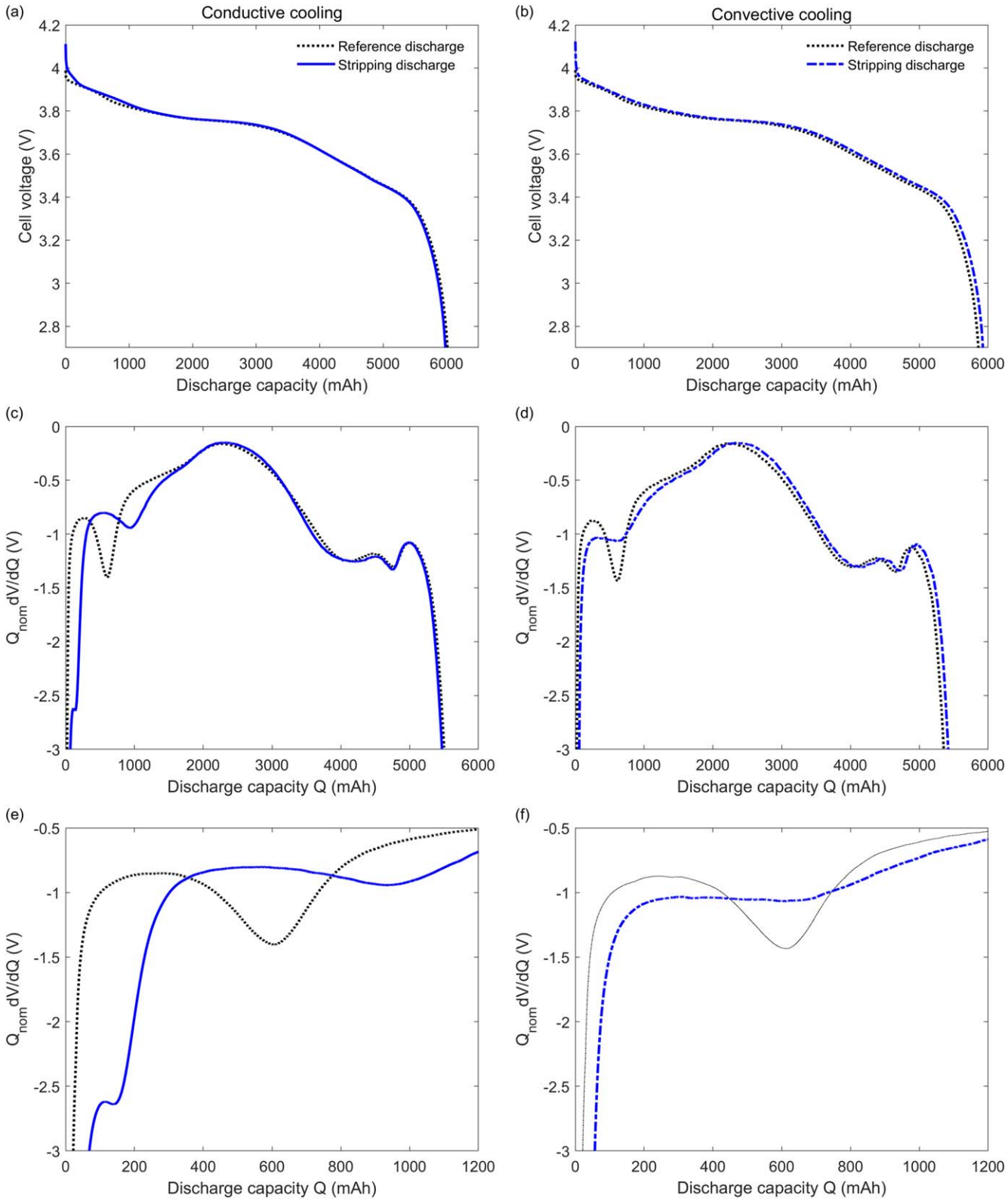

Figure 3. Experimental voltage-capacity and differential voltage (DV) measurements from Campbell et al.[6] Panel (a) shows the voltage-capacity plots for the conductively cooled cell, while panel (b) shows those for the convectively cooled cell. Panels (c) and (d) show the DV plots for the conductively cooled and convectively cooled cells respectively, i.e., the derivatives of the voltage-capacity plots above. Panels (e) and (f) show the same DV data as panels (c) and (d) respectively but zoomed in for the first 1000 mAh of discharge, when the minima of interest occur.

experiment. A later, smaller minimum at 1000 mAh has more similarity with those observed by Refs. 18–20. These minima are widely believed to correspond to the end of stripping.[17] However, Campbell et al.[6] compared their results with half-cell measurements performed by Ecker et al.[22] and concluded that the second minimum in the stripping discharge is actually a delayed version of the first

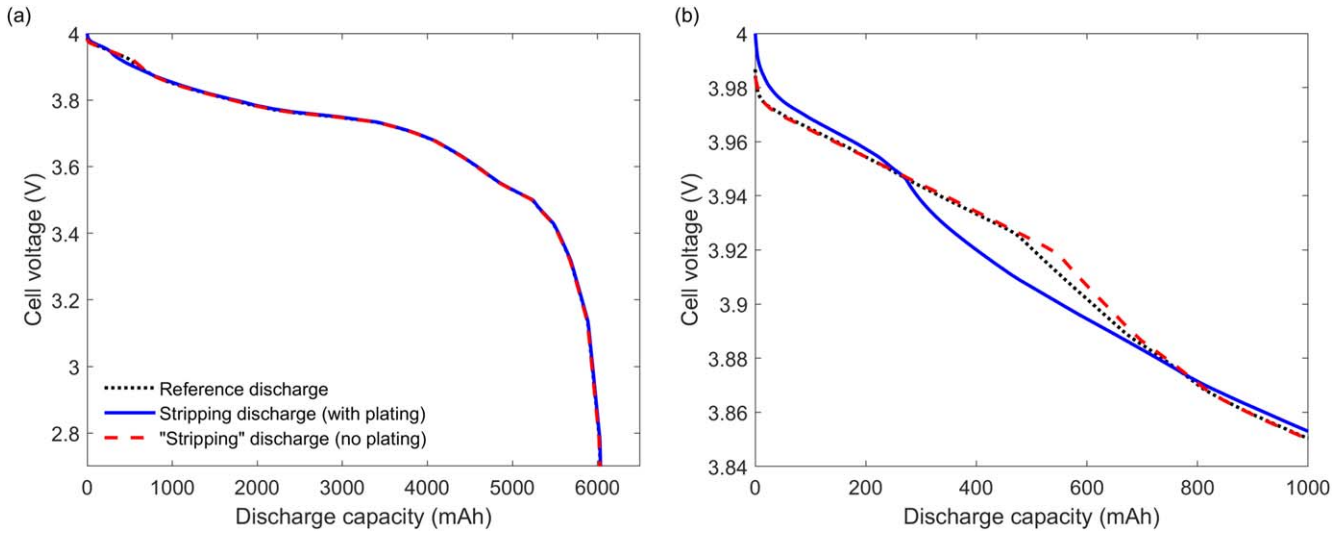

Figure 4. Simulated voltage-capacity plots for a constant temperature of 273.15 K, which corresponds to the conductively cooled cell in the experiment. Panel (a) shows the full capacity range; panel (b) zooms in on the region of interest.

minimum in the reference discharge, which is caused by a stage transition in the graphite negative electrode and not stripping. The first DV minimum, which is not present in the reference discharge, is completely absent for the convectively cooled cell. Despite this, a cell teardown confirmed the presence of metallic Li in both cells. There were no DV features in the convectively cooled cell that could be attributed to stripping, yet plating had clearly occurred, leading Campbell et al.[6] to conclude, "absence of evidence is not evidence of absence." For the convectively cooled cell, both the reference and stripping discharges have only one minimum, at 600 mAh.

Modelling provides the additional freedom to enable and disable Li plating at will, providing further insight into which features can be attributed to plating/stripping. Figure 4 shows simulated voltage-capacity plots at constant temperature $T_{\text{init}} = 273.15$ K. Two cases were modelled: one with $k_{\text{sr}} = 1 \times 10^{-10}$ m s^{-1}, which is justified below, and a control study with $k_{\text{sr}} = 0$, i.e., no plating. Panel (a) provides an overview of the full capacity range; panel (b) zooms in on the key region of interest. Inspection of panel (b) reveals that both stripping discharges also contain abrupt changes in the gradient, which occur just before 300 mAh with plating and around 600 mAh without plating.

These features are easier to identify using DV plots for the same data sets, which are shown in Fig. 5. The noise in the experimental data is not present in the simulations, but the same smoothing algorithm is applied anyway, to make comparison between simulation and experiment simpler. Panel (a) shows the full capacity range. For the case with plating, all of the maxima and minima in the experimental data shown in Fig. 3c are present in the simulated data, albeit at slightly different capacities. Panel (b) focuses on the first 1000 mAh of discharge and the features that occur in that time frame. For the case with plating, there are two minima: a large one at 285 mAh and a much smaller one at 770 mAh, which have amplitudes within 25% of the experimental minima at 140 mAh and 1000 mAh in Fig. 3e. For the case without plating, there are two broad minima at 600 and 800 mAh, which overlap so much they are almost one single minimum. A similar pair of overlapping minima is observed in the reference discharge. The effect of plating is to drive these overlapping minima apart, forming two distinct features. These results strengthen the argument of Campbell et al.[6] that the first minimum, not the second, is the indicator of plating.

While the predicted magnitude of the first DV minimum is within 25% of the experimental value, the capacity value at which it occurs

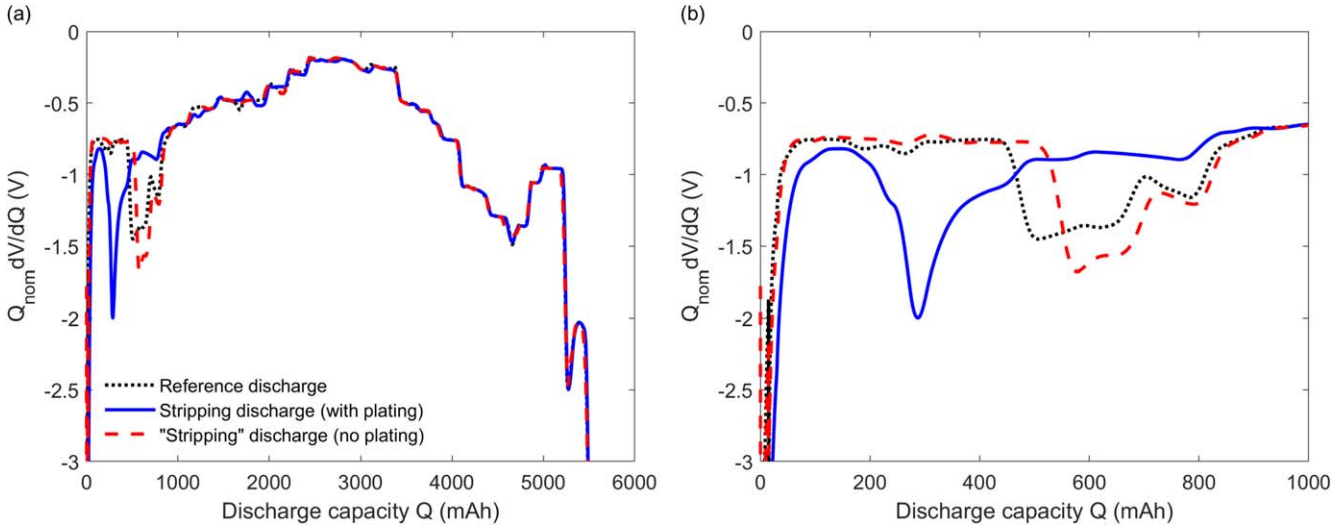

Figure 5. Simulated differential voltage (DV) plots for a constant temperature of 273.15 K, i.e., the derivatives of the data in Fig. 4. Panel (a) shows the full capacity range; panel (b) zooms in on the region of interest.

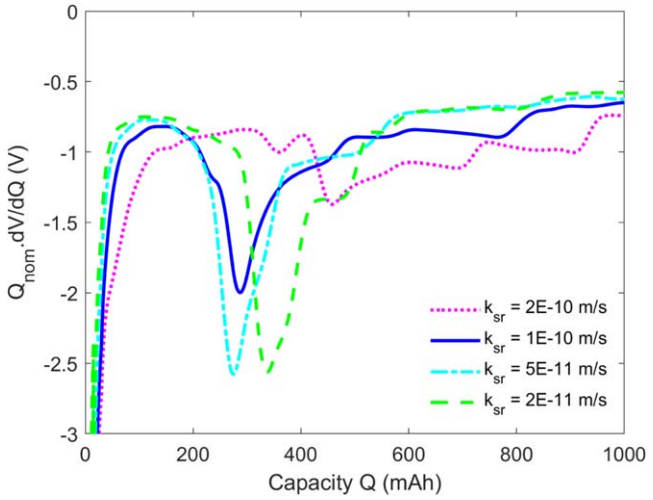

Figure 6. Simulated DV plots for a constant temperature of 273.15 K and different values of the rate constant k_{sr} for Li plating and stripping. Only the first 1000 mAh of discharge is shown. Additional plots for this study are shown in the Supplementary Information.

is double that in the experiment. One possible reason for the difference is that the values for the positive electrode utilization fraction and inactive material fraction were taken directly from Ecker et al.,[25] whereas the equivalent values for the negative electrode were adjusted to fit this particular data set (see Simulations section and Supplementary Information). Another possible reason is that this model is one-dimensional and assumes plating to be uniform across the electrode area, despite it being well-known that plating is greater at the edge of the negative electrode.[6,7] In addition, despite the cell surface being at a constant temperature, there may have been thermal gradients within the cell that the model does not account for.

Since no technique for measuring k_{sr} has been proposed, let alone any measurements been carried out, k_{sr} is treated as an adjustable fitting parameter. Figure 6 shows simulated DV plots for different values of k_{sr}, this time focusing only on the first 1000 mAh of discharge and only showing stripping discharges. The initial large minimum is present for all four k_{sr} values. For $k_{sr} = 2 \times 10^{-10}$ m s^{-1} there are two additional minima after the large one and a small minimum before, for $k_{sr} = 1 \times 10^{-10}$ m s^{-1} there is one additional minimum after the large one and for smaller k_{sr} values only one minimum is present, followed by a plateau. Only $k_{sr} = 1 \times 10^{-10}$ m s^{-1} results in the same number of minima as observed in the experiment, so this value is used throughout this study. Further analysis and discussion of these reuslts, including an explanation of the underlying physics, can be found in the Supplementary Information.

A similar simulation was done for the cell with self-heating during charge and slow cooling during discharge, governed by 13 and 14 respectively, to correspond with the experiment with natural air convection. Figure 7 shows similar voltage-capacity plots to Fig. 4 for the cell with self-heating. The abrupt gradient changes in the constant temperature simulation also occur here, but at lower discharge capacities: around 200 mAh with plating and 500 mAh without plating.

Figure 8 shows the DV plots for the simulation with self-heating. As with the constant temperature simulation, all maxima and minima in the experiment are reproduced in the case with plating. Unlike in the experimental measurement, the large minimum close to the beginning of discharge is still present in the stripping discharge with plating but is now moved to 210 mAh. The broad, overlapping minima in the reference discharge are also still present, while the second minimum in the stripping discharge is shifted to 600 mAh and is barely visible.The model is unable to explain why the first DV minimum is absent for the convectively cooled experimental cell. However, the second minimum is predicted to occur at the same capacity as in the experiment. The amplitude of the second minimum is again predicted to within 25% of the experimental value.

The extent of plating in the simulated cells can be quantified by calculating the total capacity Q_{Li} of plated Li, which involves integrating the plated Li concentration c_{Li} over the volume v of the negative electrode and multiplying by Faraday's constant F:

$$Q_{Li} = F \int_v c_{Li}\ \mathrm{d}v = FA \int_0^{\delta_-} c_{Li}\ \mathrm{d}x, \qquad [15]$$

where $A = 0.41208$ m^2[25] is the total planar electrode area. Figure 9 shows the decline of Q_{Li} during the stripping discharge. The DV minima, which are widely believed to mark the end of stripping, are observed at 285 mAh and 210 mAh for the constant temperature and self-heating simulations respectively. However, lithium stripping continues until after 2500 mAh. Therefore, the minima in these simulations clearly do not indicate the end of stripping, but do appear to indicate that stripping is occurring.

To investigate the physical mechanism that causes these minima, it is helpful to calculate the average values of the normalized surface concentration $c_s^* = \frac{c_s}{c_{m-}}$ and open-circuit potential $U_-(c_s^*)$ across the thickness of the negative electrode:

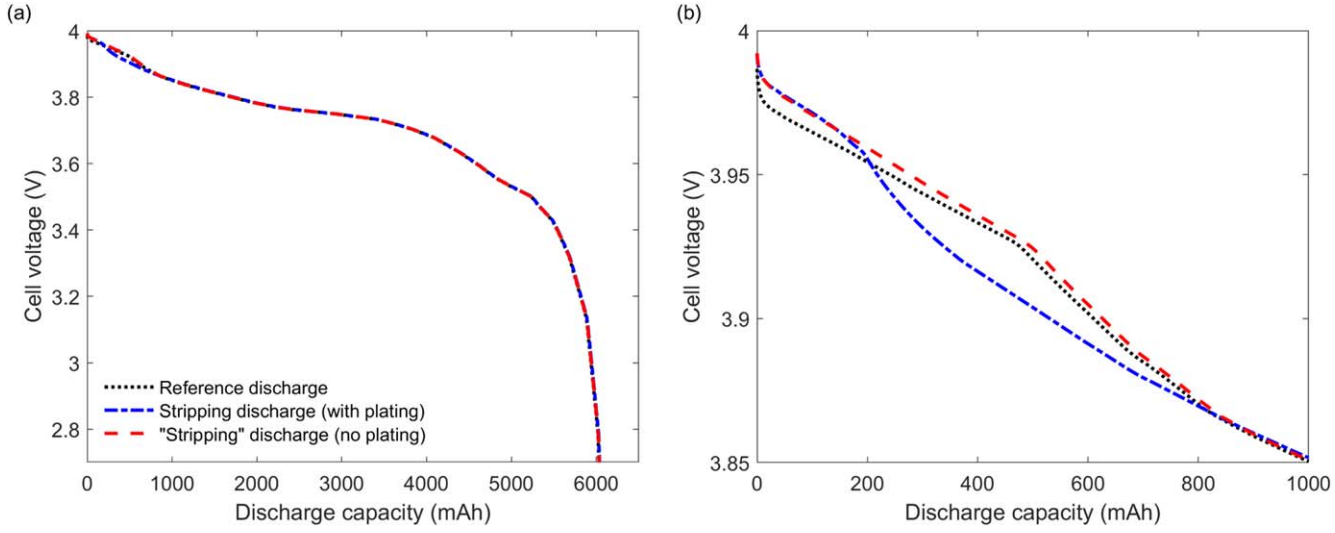

Figure 7. Simulated voltage-capacity plots with self-heating during charge and cooling during discharge, which corresponded to the convectively cooled cell in the experiment. Panel (a) shows the full capacity range; panel (b) zooms in on the region of interest.

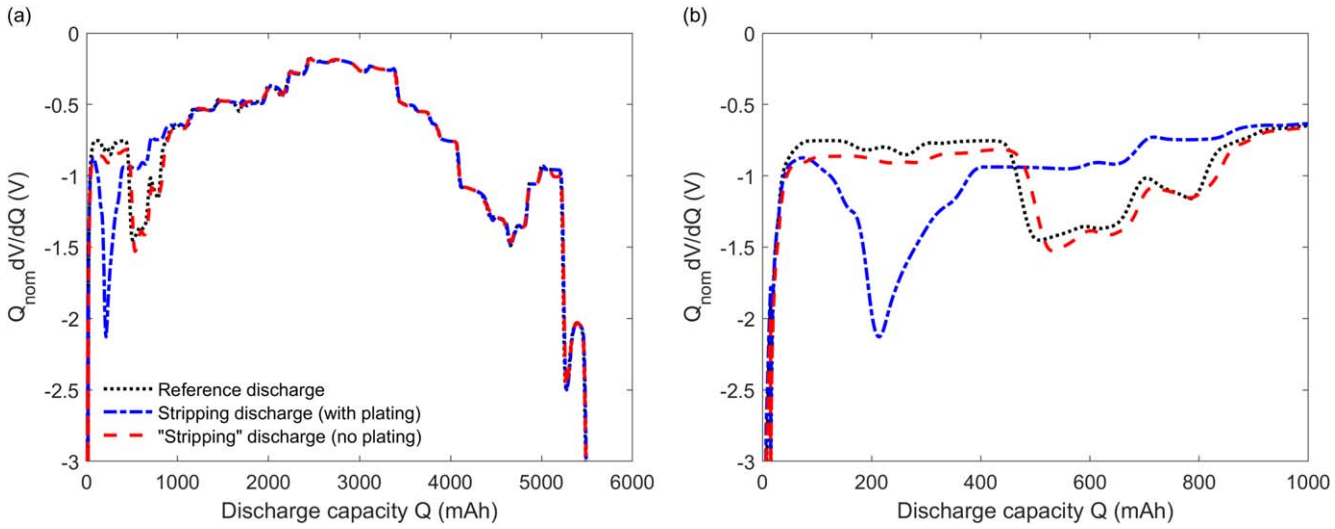

Figure 8. Simulated DV plots with self-heating during charge and cooling during discharge, i.e., the derivatives of the data in Fig. 7. Panel (a) shows the full capacity range; panel (b) zooms in on the region of interest.

$$\langle c_s^* \rangle(t) = \frac{1}{\delta_-} \int_0^{\delta_-} c_s^* \, \mathrm{d}x \qquad [16]$$

$$\langle U_- \rangle(t) = \frac{1}{\delta_-} \int_0^{\delta_-} U_-(c_s^*) \mathrm{d}x. \qquad [17]$$

Figure 10a shows $\langle c_s^* \rangle(t)$ for the first 1000 mAh of discharge for the constant temperature simulation, while Fig. 10b shows $\langle U_- \rangle(t)$ over the same period. By comparing these plots with Fig. 1a, the cause of the DV minima becomes clear: the stage II-stage III phase transition is triggered after 270 mAh of discharge with plating and 550 mAh without plating. The reason the surface concentration decreases faster when stripping is present is that the occurrence of plating results in less Li being available to intercalate into graphite. The surface of the graphite particles is still almost fully lithiated after the fast charge but there is less Li available overall, causing a shortage of Li in the centre of the particles. This large concentration gradient between the centre and surface of the particles drives rapid diffusion of Li from surface to centre, causing the stage II-stage III phase transition to occur sooner and more abruptly than it would with no plating. The DV minimum therefore occurs sooner and more abruptly as well. After the secondary minima around 800 mAh, all three $\langle U_- \rangle(t)$ curves become flat again, meaning the phase transition has ended. The DV is not zero when $\langle U_- \rangle(t)$ is flat because of the remaining contribution from the positive electrode ($U_+(c_a^*)$ is plotted in the Supplementary Information).

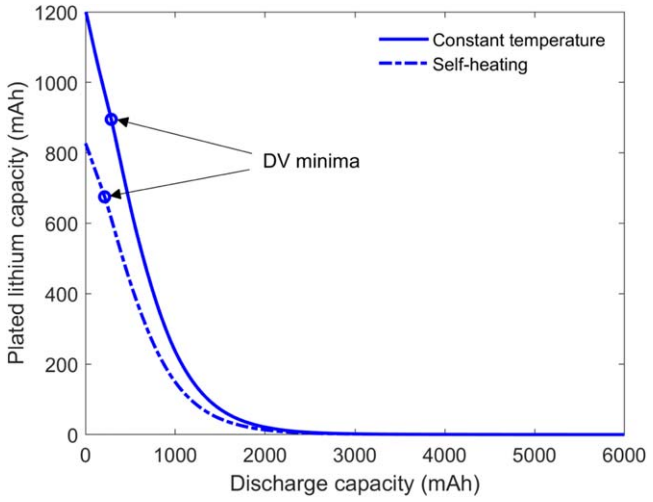

Figure 9. Capacity of plated Li for both the simulation with constant temperature and that with self-heating. The circles indicate the capacities at which the DV minima in Figs. 5c and 8c occur.

In order to test the hypothesis that the first DV minimum is caused by an early phase transition, another constant temperature simulation was conducted with constant diffusion coefficients. The constant diffusion coefficients were obtained by performing an average over all values of $D_\pm(c_a^*)$:

$$\langle D_\pm \rangle = \int_0^1 D_\pm(c_a^*) \mathrm{d}c_a^*, \qquad [18]$$

resulting in $\langle D_- \rangle = 2.1 \times 10^{-14}$ m^2 s^{-1} in the negative electrode and $\langle D_+ \rangle = 1.5 \times 10^{-13}$ m^2 s^{-1} in the positive electrode, which have the same orders of magnitude as those used by Ren et al.[19] In the graphite negative electrode, use of 18 means the diffusion far from phase transitions will be significantly faster than for the concentration-dependent diffusion depicted in Fig. 1b, while the opposite will be true at the phase transitions themselves (note that $U_\pm$ is still concentration-dependent).

Figure 11a shows DV plots with constant diffusion coefficients $\langle D_\pm \rangle$, a constant temperature of 273.15 K and different values of k_{sr}, focusing on the first 1000 mAh only. Unlike in the simulations with nonlinear diffusion, the reference discharges are not identical, so they are plotted as thin black lines while the stripping discharges are plotted as thick coloured lines. With the averaged diffusion coefficients, the first DV minimum disappears. On increasing k_{sr} by a factor of 200, the minimum reappears at a discharge capacity of 77 mAh. Figures 11b and 11c show the corresponding $\langle c_s^* \rangle(t)$ and $\langle U_- \rangle(t)$. The phase transition in Fig. 11c does not line up with the DV minimum in panel (a), so another explanation for the DV minimum is sought. Figure 11d, which plots the average overpotential $\langle \eta \rangle(t)$ in the negative electrode, shows a steep gradient in the same capacity range as the DV minimum.

The capacity Q_{Li} of plated lithium for the simulation with averaged diffusion coefficients is plotted in Fig. 12. For $k_{sr} = 2 \times 10^{-8}$ m s^{-1}, Li stripping is mostly complete, though not entirely, when the DV minimum occurs; Yang et al.[18] made a similar finding. The sharp overpotential gradient therefore occurs during the period when the dominant reaction switches from stripping to deintercalation; the overpotential rises to allow deintercalation to occur.

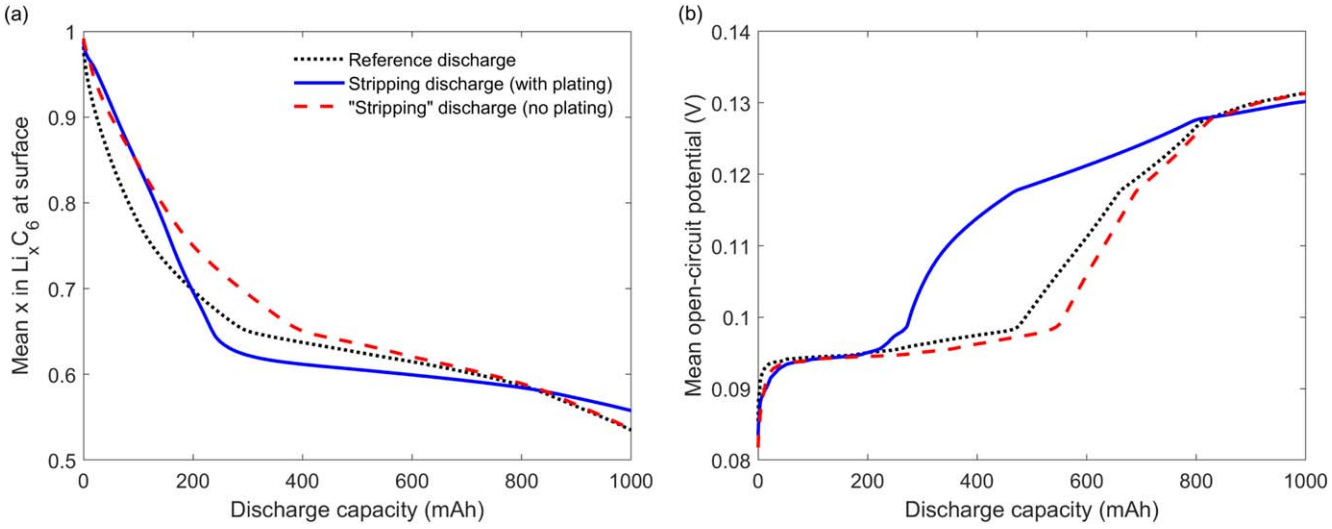

Figure 10. Mean values of (a) normalized Li^+ concentration at the particle surface and (b) resulting open-circuit potential, averaged over the graphite negative electrode, during the constant temperature simulation.

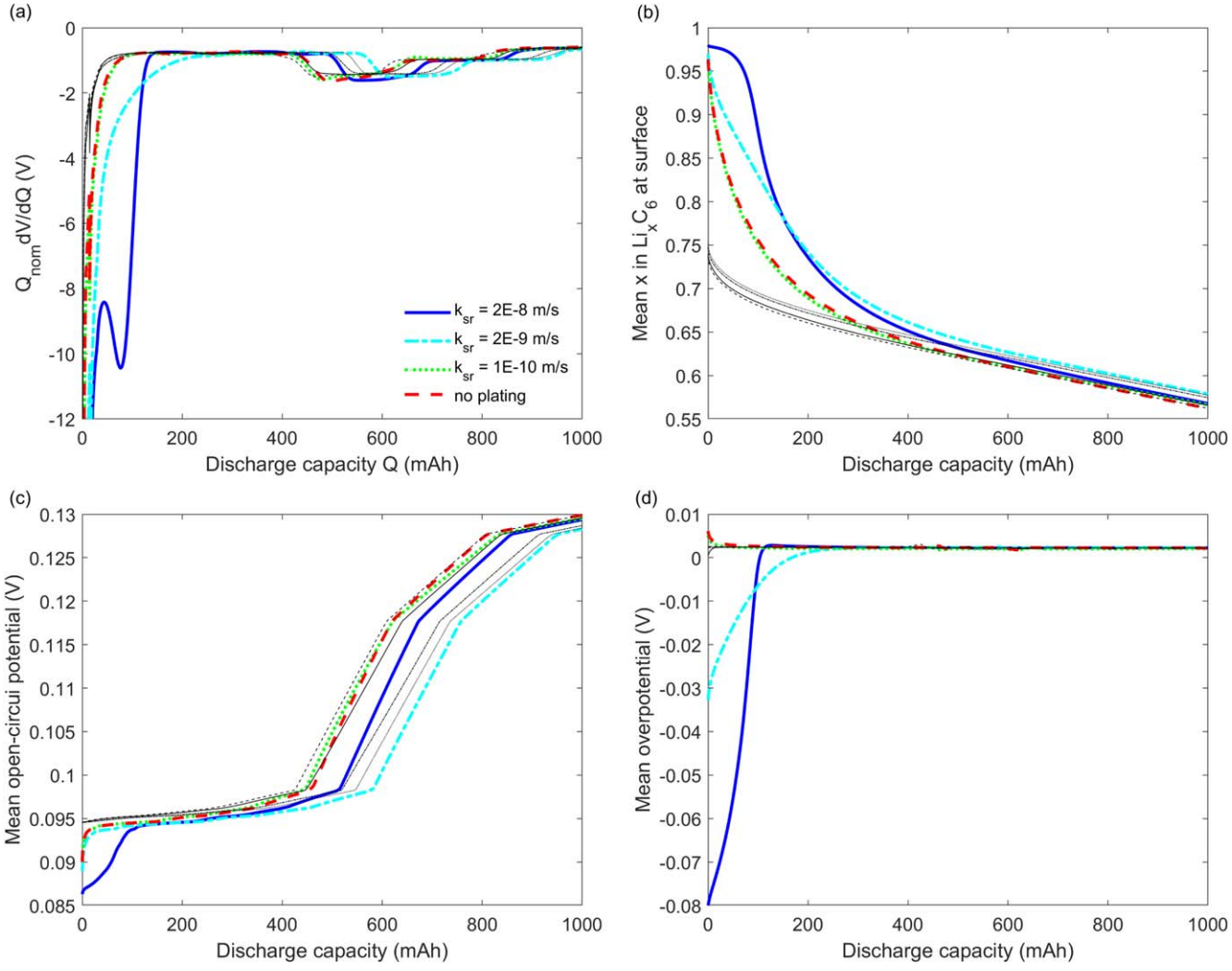

Figure 11. Results of the simulation with constant temperature, concentration-independent diffusion coefficients in the electrode particles and different values of the rate constant k_{sr} for Li plating and stripping. Thin black lines are reference discharges; thick coloured lines are stripping discharges. Panel (a) shows the DV plots, while panels (b), (c) and (d) show the mean values of the normalized Li^+ surface concentration, open-circuit potential and overpotential respectively, averaged over the graphite negative electrode.

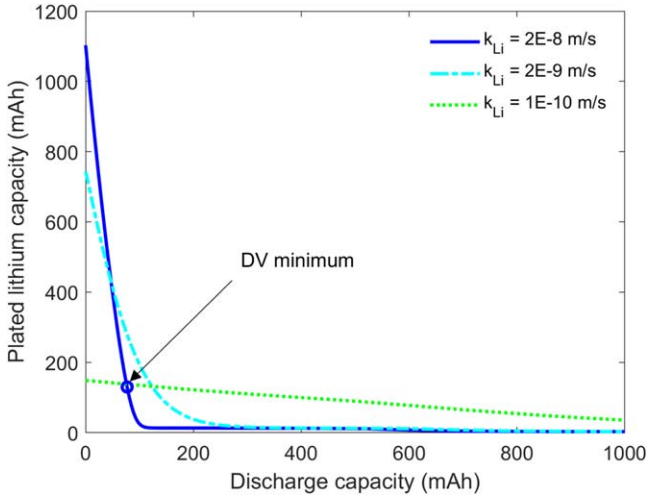

Figure 12. Capacity of plated Li for the simulation with constant temperature, concentration-independent diffusion coefficients in the electrode particles and different values of the rate constant k_{sr} for Li plating and stripping. The circle indicates the capacity at which the DV minimum occurs.

The mechanism causing the DV minimum is therefore different in the simulations with nonlinear and linear diffusion. For nonlinear diffusion, the minimum is caused by a phase transition in the graphite and Li stripping persists for over 2000 mAh afterwards. For linear diffusion, the higher k_{sr} means that stripping is mostly completed by the time the minimum is observed, forcing the overpotential η to shift to a value favouring the deintercalation reaction, thus causing the DV minimum that way.

There are therefore two possible explanations for the DV minimum commonly observed after a fast charge. The dominant explanation in the literature is that the minimum marks the end of Li stripping and can therefore be used as a means of quantifying the amount of Li plated after a single fast charge. The simulations in this work suggest that if the diffusion coefficient of Li^+ intercalated in graphite is not sensitive to phase transitions, the minimum does indeed mark the end of stripping. However, the literature shows that the diffusion coefficient is highly sensitive to phase transitions.[21–24] As a result, the simulations predict that Li stripping is much slower and the minimum is caused by the stage II-stage III phase transition instead. Lithium plating causes this phase transition to begin sooner and more abruptly than it would otherwise, causing the DV minimum associated with the phase transition to be split into two.

There are two possible reasons why the DV minimum splitting is not observed in the experiment where the cell was cooled by natural convection. Either the splitting does not occur, or it does occur but the first minimum is moved to such a low capacity value that it cannot be resolved experimentally. The low amplitude of the second minimum, compared to the reference discharge, is consistent with the second possibility. A possible cause for such extreme splitting is that the extent of self-heating is underestimated by the surface temperature measurements and the core temperature during the experiment is in fact greater. In this case, plating would still occur causing large concentration gradients inside the graphite particles, but rapid diffusion following self-heating would cause the phase transition to begin almost immediately after the start of discharge, resulting in an early DV minimum that would be difficult to resolve experimentally.

Conclusions

The theory that the DV minimum marks the end of Li stripping rests on the assumption that the diffusion coefficient of Li^+ in graphite has little or no dependence on Li^+ concentration. The literature shows on the contrary that the diffusion coefficient is highly sensitive to phase transitions.[21–24] In this case, the minimum is caused by plating-induced early onset of the stage II-stage III phase transition and cannot be used to quantify plating.

The model of Li plating and stripping presented in this paper is similar to that of Yang et al.[18] but contains two important differences. The first main difference is that this paper utilizes two different types of control study so that each discharge is simulated three times: once after a slow charge, once after a fast charge (stripping discharge) and once after a fast charge with plating disabled. This approach allows users to identify which features of the simulation results are due to Li plating, which are due to fast charging and which would occur even with no fast charge. The results strengthen the argument of Campbell et al.[6] that the DV minimum observed at just over 10% of discharge capacity is not caused by Li stripping, while an earlier minimum is.

The second and more important innovation is the use of concentration-dependent diffusion coefficient data from Ecker et al.[22] that explicitly accounts for phase transitions in the graphite negative electrode, in accordance with earlier findings.[21,23,24] The effect of diffusion in the electrode particles was studied in two ways: by varying the temperature, mimicking conductive and convective cooling scenarios, and by replacing the concentration-dependent diffusion coefficient with a constant value. The DV features observed at the beginning of discharge in the constant temperature simulation were also observed in the self-heating simulation, but earlier in the discharge due to faster diffusion in graphite.

When the concentration-dependent diffusion coefficient was removed and the diffusion equation therefore made linear, the DV minimum disappeared. Increasing the rate constant k_{sr} for plating/stripping by a factor of 200 retrieves the minimum, but the mechanism causing it is changed so that stripping is mostly completed when the minimum is observed.

Model predictions show that an unusually sharp DV minimum at the beginning of discharge could be evidence of Li plating, while the associated experiments[6] found that Li plating can occur even if no sharp DV minimum is observed. This knowledge does not rule out DV analysis as a diagnostic technique for detecting Li plating, but casts doubt on its reliability.

A major weakness of all electrochemical models of Li plating is the lack of any experimental procedure for measuring the constant k_{sr} governing the plating/stripping reaction. If this becomes available, the models will become more physically realistic and a major advance in understanding Li plating/stripping will almost certainly result.

Acknowledgments

The authors would like to acknowledge financial support from EPSRC Faraday Institution Multiscale Modelling project (EP/S003053/1, grant number FIRG003).

ORCID

Simon E. J. O'Kane https://orcid.org/0000-0003-3141-1657
Ian D. Campbell https://orcid.org/0000-0002-5465-6449
Gregory J. Offer https://orcid.org/0000-0003-1324-8366
Monica Marinescu https://orcid.org/0000-0003-1641-3371

References

1. A. Tomaszewska et al., "Lithium-ion battery fast charging: a review." *eTransportation*, **1**, 100011 (2019).
2. J. Sieg, J. Bandlow, T. Mitsch, D. Dragicevic, T. Materna, B. Spier, H. Witzenhausen, M. Ecker, and D. U. Sauer, "Fast charging of an electric vehicle lithium-ion battery at the limit of the lithium deposition process." *Journal of Power Sources*, **427**, 260 (2019).
3. A. M. Colclasure, A. R. Dunlop, S. E. Trask, B. J. Polskin, A. J. Jansen, and K. Smith, "Requirement for enabling extreme fast charging of high energy Li-ion cells while avoiding lithium plating." *Journal of the Electrochemistry Society*, **166**, A1412 (2019).
4. J. Vetter, P. Novák, M. R. Wagner, C. Veit, K.-C. Möller, J. O. Besenhard, M. Winter, M. Wohlfahrt-Mehrens, C. Vogler, and A. Hammouche, "Ageing mechanisms in lithium-ion batteries." *Journal of Power Sources*, **147**, 269 (2005).

5. P. Arora, M. Doyle, and R. E. White, "Mathematical modelling of the lithium deposition overcharge reaction in lithium-ion batteries using carbon-based negative electrodes." *Journal of the Electrochemistry Society*, **146**, 3453 (1999).
6. I. D. Campbell, M. W. J. Marzook, M. Marinescu, and G. J. Offer, "How observable is lithium plating? Differential voltage analysis to identify and quantify lithium plating following fast charging of cold lithium-ion batteries." *Journal of the Electrochemistry Society*, **166**, A725 (2019).
7. M. Tang, P. Albertus, and J. Newman, "Two-dimensional modeling of lithium deposition during cell charging." *Journal of the Electrochemistry Society*, **156**, A390 (2009).
8. C.-S. Kim, K. M. Jeong, K. Kim, and C.-W. Yi, "Effects of capacity ratios between anode and cathode on electrochemical properties for lithium polymer batteries." *Electrochimica Acta*, **155**, 431 (2015).
9. P. Bai, J. Li, F. R. Brushett, and M. Z. Bazant, "Transition of lithium growth mechanisms in liquid electrolytes." *Energy Environ. Sci.*, **9**, 3221 (2016).
10. A. Kushima, K. P. So, C. Su, P. Bai, N. Kuriyama, T. Maebashi, Y. Fujiwara, M. Z. Bazant, and J. Li, "Liquid cell transmission electron microscopy observation of lithium metal growth and dissolution: root growth, dead lithium and lithium flotsams." *Nano Energy*, **32**, 271 (2017).
11. K.-H. Chen, K. N. Wood, E. Kazyak, W. S. LePage, A. L. Davis, A. J. Sanchez, and N. P. Dasgupta, "Dead lithium: mass transport effects on voltage, capacity, and failure of lithium metal anodes." *Journal of Materials Chemistry A*, **5**, 11671 (2017).
12. X.-G. Yang, Y. Leng, G. Zhang, S. Ge, and C.-Y. Wang, "Modeling of lithium plating induced aging of lithium-ion batteries: transition from linear to nonlinear aging." *Journal of Power Sources*, **360**, 28 (2017).
13. S. Santhanagopalan, P. Ramadass, and J. (Zhengming) Zhang, "Analysis of internal short-circuit in a lithium ion cell." *Journal of Power Sources*, **194**, 550 (2009).
14. Y. Zhang, X. Li, L. Su, Z. Li, B. Liaw, and J. Zhang, "Lithium plating detection and quantification in Li-ion cells from degradation behaviours." *ECS Trans.*, **75**, 37 (2017).
15. T. Waldmann, M. Wilka, M. Kasper, M. Fleischhammer, and M. Wohlfahrt-Mehrens, "Temperature dependent ageing mechanisms in lithium-ion batteries - a post-mortem study." *Journal of Power Sources*, **262**, 129 (2014).
16. M. C. Smart, B. V. Ratnakumar, L. Whitcanack, K. Chin, M. Rodriguez, and S. Surampudi, "Performance characteristics of lithium ion cells at low temperatures." *IEEE Aerospace and Electronic Systems Magazine*, **17**, 16 (2002).
17. M. Petzl and M. A. Danzer, "Nondestructive detection, characterization, and quantification of lithium plating in commercial lithium-ion batteries." *Journal of Power Sources*, **254**, 80 (2014).
18. X.-G. Yang, S. Ge, T. Liu, Y. Leng, and C.-Y. Wang, "A look into the voltage plateau signal for detection and quantification of lithium plating in lithium-ion cells." *Journal of Power Sources*, **395**, 251 (2018).
19. D. Ren, K. Smith, D. Guo, X. Han, X. Feng, L. Lu, and M. Ouyang, "Investigation of lithium plating-stripping process in Li-ion batteries at low temperature using an electrochemical model." *Journal of the Electro-chemistry Society*, **165**, A2167 (2018).
20. X. Zhao, Y. Yin, Y. Hu, and S.-Y. Choe, "Electrochemical-thermal modeling of lithium plating/stripping of $Li(Ni_{0.6}Mn_{0.2}Co_{0.2})O_2$/carbon lithium-ion batteries at subzero ambient temperatures." *Journal of Power Sources*, **418**, 61 (2019).
21. M. D. Levi and D. Aurbach, "Diffusion coeffcients of lithium ions during intercalation into graphite derived from the simultaneous measurements and modeling of electrochemical impedance and potentiostatic intermittent titration characteristics of thin graphite electrodes." *J. Phys. Chem. B*, **101**, 4641 (1997).
22. M. Ecker, T. K. D. Tran, P. Dechent, S. Käbitz, A. Warnecke, and D. U. Sauer, "Parameterization of a physico-chemical model of a lithium-ion battery I. determination of parameters." *Journal of the Electrochemistry Society*, **162**, A1836 (2015).
23. K. Persson, V. A. Sethuraman, L. J. Hardwick, Y. Hinuma, Y. S. Meng, A. van der Ven, V. Srinivasan, R. Kostecki, and G. Ceder, "Lithium dffusion in graphitic carbon." *The Journal of Physical Chemistry Letters*, **1**, 1176 (2010).
24. D. R. Baker and M. W. Verbrugge, "Intercalate diffusion in multiphase electrode materials and application to lithiated graphite." *J. Electrochem. Soc.*, **159**, A1341 (2012).
25. M. Ecker, S. Käbitz, I. Laresgoiti, and D. U. Sauer, "Parameterization of a physico-chemical model of a lithium-ion battery II. model validation." *Journal of the Electrochemistry Society*, **162**, A1849 (2015).
26. T. F. Fuller, M. Doyle, and J. Newman, "Simulation and optimization of the dual lithium ion insertion cell." *Journal of the Electrochemistry Society*, **141**, 1 (1994).
27. M. W. Verbrugge and B. J. Koch, "Microelectrode investigation of ultrahigh-rate lithium deposition and stripping." *Journal of Analytical Chemistry*, **367**, 123 (1994).
28. K. N. Wood, E. Kazyak, A. F. Chadwick, K.-H. Chen, J.-G. Zhang, K. Thornton, and N. P. Dasgupta, "Dendrites and pits: untangling the complex behavior of lithium metal anodes through operando video microscopy." *ACS Central Science*, **2**, 790 (2016).
29. M. W. Verbrugge and B. J. Koch, "Microelectrode study of the Lithium/Propylene carbonate interface: temperature and concentration dependence of physicochemical parameters." *J. Electrochem. Soc.*, **141**, 3053 (1994).
30. C. A. Paddon, S. E. W. Jones, F. L. Bhatti, T. J. Donohoe, and R. G. Compton, "Kinetics and thermodynamics of the Li/Li+ couple in tetrahydrofuran at low temperatures (195–295 K)." *Journal of Physical Organic Chemistry*, **20**, 677684 (2007).
31. R. Wibowo, S. E. W. Jones, and R. G. Compton, "Kinetic and thermodynamic parameters of the Li/Li+ couple in the room temperature ionic liquid N-Butyl-N-methylpyrrolidinium Bis(trifluoromethylsulfonyl) imide in the temperature range 298–318 K: a theoretical and experimental study using Pt and Ni electrodes." *J. Phys. Chem. B*, **113**, 12293 (2009).
32. R. Tao, X. Bi, S. Li, Y. Yao, F. Wu, Q. Wang, C. Zhang, and J. Lu, "Kinetics tuning the electrochemistry of lithium dendrites formation in lithium batteries through electrolytes." *ACS Appl. Mater. Interfaces*, **9**, 7003 (2017).
33. G. Sikha, B. N. Popov, and R. E. White, "Effect of porosity on the capacity fade of a lithium-ion battery." *Journal of the Electrochemistry Society*, **151**, A1104 (2004).
34. B. Gyenes, D. A. Stevens, V. D. Chevrier, and J. R. Dahn, "Understanding anomalous behavior in coulombic effciency measurements on Li-ion batteries." *Journal of the Electrochemistry Society*, **162**, A278 (2015).